Positive magnetoresistance induced by fan-type phases in a spin-spiral magnet

L. Benito,[1,*] R. C. C. Ward,[2] and M. G. Blamire[1]

[1]*Department of Material Science and Metallurgy, Cambridge University, Pembroke Street, Cambridge CB2 3QZ, United Kingdom*

[2]*Oxford Physics, Clarendon Laboratory, Parks Road, University of Oxford, Oxford OX1 3PU, United Kingdom*

(Received 28 September 2012; published 6 December 2013)

We report on the positive magnetoresistance (MR) that accompanies the onset of fan-type magnetic structures in an epitaxially grown Dy/Y superlattice (SL). We find that MR ratios for current perpendicular to plane (CPP) and in-plane (CIP) geometries yield comparable values and a similar nonmonotonic dependence on the applied magnetic field H and temperature, which result in a maximum MR $\sim 0.45\%$ at $T = 110$ K. We demonstrate that the rise in resistance is due to the increase in the number of superzone band gaps that accompanies the magnetization process of the anisotropic spin-spiral magnet, which reflects on the increasing complexity of the field-induced modulated magnetic structures. Furthermore, we find that the suppression of the giant MR in Dy/Y SL is due mainly to the combined action of chemical modulation and epitaxial strain effects. Finally, MR presents a linear (negative slope) and unsaturated scaling with H in the magnetized state, which is a clear fingerprint of magnon MR in highly anisotropic magnetic materials.

DOI: 10.1103/PhysRevB.88.224407 PACS number(s): 75.30.Gw, 75.50.Cc, 75.70.Cn

I. INTRODUCTION

A promising trend in spintronics consists of exploring new effects that arise when a spin-polarized current travels through inhomogeneous magnetic media.[1] To this regard, heavy rare-earth (RE) metals—prototypes of spin-spiral magnetic phases[2,3]—have been pointed out as potential materials for testing novel magnetoelectric phenomena. Thus, for instance, Robinson *et al.*,[4] has recently demonstrated the controlled injection of spin-triplet supercurrents into a strong ferromagnet. In addition, an early chiral asymmetry effect predicted in magnetic multilayers[5] has been more recently found in a Dy/Y (Ref. 6) superlattice (SL). This result suggests that chiral RE-based heterostructures are potential candidates for exploring the electrical magneto-chiral anisotropy[7] effect, which has sparked off renovated interest in the magnetotransport properties of RE-based thin films and multilayers.

The onset of magnetic order among the localized $4f$ electrons in lanthanides is accomplished through the mediation of the conduction electrons (CEs) by means of an indirect-exchange[8] interaction or Ruderman-Kittel-Kasuya-Yosida[9] (RKKY) coupling mechanism. In this way, the Bragg scattering of the CEs by the magnetic lattice results in new Brillouin zone (BZ) boundaries,[10] which entail the wipe-off of large areas of the Fermi surface (FS) topology by the emergence of superzone band gaps,[10] resulting in a sharp upturn in the resistivity[11,12] upon the magnetic ordering transition. An applied magnetic field suppresses the *superzones*, which results in a giant magnetoresistance[13,14] (GMR), for instance, this amounts to $\sim$16% in bulk Dy.[12] Contrary to GMR phenomena in $3d$-based multilayers,[15] MR in RE metals is regarded as a genuine *bulk effect*,[10] which potentially opens up the possibility to optimize the magnetotransport in RE-based systems by engineering the epitaxial strain and/or chemical modulation. However, gaining a better understanding of spin-dependent transport in RE-based nanostructures is central prior to embark in exploring novel spintronics effects in noncollinear nanomagnets.

According to Elliott *et al.*,[16] magnetoelectric theory, thereafter EW theory, the spin-dependent scattering mechanism[10] in RE metals is formulated in terms of the *spin-disorder*[17] model, so that, $4f$ spins are regarded as uncorrelated scattering centers. In this context, the field-dependent resistivity can be written as

$$\frac{\Delta\rho}{\rho_0} = -A\frac{M^2(T,H)}{M_s^2(T)}, \tag{1}$$

where $\Delta\rho = \rho_H - \rho_0$, ρ_H is the field-dependent resistivity, $\rho_0 = \rho_{H=0}$, M is the field-dependent magnetization, and M_s is the saturation magnetization. Equation (1) predicts a negative MR as the applied magnetic field H rises, in agreement with modulated collinear structures.[13,18] However, in spin-spiral magnets, the field-induced suppression of the *superzones* yields an unexpected positive MR in the low-field limit and a puzzling nonmonotonic scaling of MR[19,20] with H, in clear disagreement with EW[16] theory. Unlocking the mechanism by which positive MR sets in helical magnets is a quest of fundamental interest in noncollinear spintronics.

We report on a combined magnetotransport and magnetization study in a helical RE-based SL, which shows that the positive MR in spin-spiral magnets is linked to the onset of distorted spin-spiral and fan-type magnetic structures. We observe that MR becomes isotropic in the Dy/Y SL, so that, current in-plane (CIP) and perpendicular to plane (CPP) MR attain very similar values, and both present a nonmonotonic scaling with H and T. More importantly, we demonstrate that the rise in MR is originated in the appearance of a large number of superzone band gaps, which reflects on the field-induced enrichment of the Fourier spectrum of distorted helix and fan-type magnetic structures. We finally show that the linear and unsaturated scaling of the high-field MR is due to the scattering of conduction electrons by spin waves.

The structure of the paper goes as follows. A brief description of sample's deposition, device nanofabrication, and magnetization and resistivity measurements is given in Sec. II. A summary of samples's x-ray diffraction characterization, magnetometric measurements, including a magnetic phase diagram, and a discussion of the magnetoelectric measurements is presented in Sec. III. In Sec. IV, we have extended EW theory

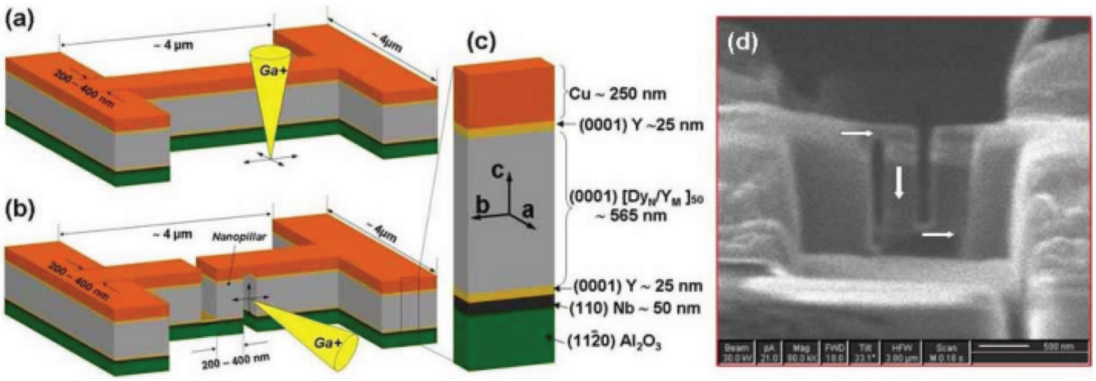

FIG. 1. (Color online) Sketch of the pillarlike nanodevice fabrication using a focused ion beam (FIB) microscope as a nanomilling tool. (a) The central track of the lithographed pattern, which is 4-μm wide, is narrowed down using the FIB with beam at 90° with respect to the surface sample plane. (b) Subsequently, the sample is rotated towards an angle of 85° with respect to the surface normal and then two lateral cuts are taken—sculpting the nanodevice into a pillarlike shape, which defines the electrical current path. (c) Detail of the different layers making up the multilayered superstructure. From bottom to top: *A* plane Al_2O_3 substrate, (110)Nb buffer and (0001)Y seed layers, (0001)$[Dy_{26\pm1}/Y_{14\pm1}]_{50}$ superlattice, where 26 ± 1 and 14 ± 1 are the Dy and Y layer thickness in monolayers, respectively, and (0001)Y capping and Cu layers. (d) An FIB image of a $Nb_{50\,nm}/Y_{25\,nm}/[Dy_{26\pm1}/Y_{14\pm1}]_{50}/Y_{25\,nm}/Cu_{250\,nm}$ nanopillar device view from an angle of 33.1° from the normal to the sample plane. The nanopillar has a cross-section area of 310 nm × 330 nm. The white arrows indicate the path for the electric current through the nanopillar device. The white scale bar at the bottom-right side represents 0.5 μm.

to account for the unexpected positive magnetoresistance in helical magnets. Finally, a discussion of the likely factors that may affect the superzone effect at the nanoscale is provided in Sec. V.

II. EXPERIMENTAL METHODS

We have examined a *c*-grown $[Dy_{26\pm1}/Y_{14\pm1}]_{50}$ superlattice (SL)—thereafter referred as Dy/Y SL—grown by a molecular beam epitaxy technique onto a heated (11$\bar{2}$0) Al_2O_3 oriented substrate under ultrahigh vacuum (UHV) conditions, base pressure $P < 2 \times 10^{-10}$ mbar, where the subindexes 26 ± 1 and 14 ± 1 indicate the number of monolayers (MLs) of Dy and Y layers, respectively, and 50 is the number of repetitions of the Dy/Y unit biblock in the SL. Prior to deposition of the Dy/Y multilayer, a (110) Nb buffer and a (0001) Y seed layers—50-nm- and 25-nm-thick, respectively—were deposited. Further details can be found elsewhere.[21]

Magnetization and electrical measurements were carried out in a Cryogenic© Ltd high-field measurement system, fitted with commercial vibrating sample magnetometer and resistivity probes. Magnetization and resistivity data were collected, such as **H** is applied along the easy direction for the magnetization *M* in Dy, that is, **H**||**a**. The zero-field-cooled (ZFC) *M*-*T* curve were carried out in a Quantum Design SQUID magnetometer under the same conditions stated above. *M*-*H* and *M*-*T* data were collected in the as-grown Dy/Y SL. Magnetoelectric transport measurements were carried out by wire-bonding electrical contacts on the sample surface, using a standard four-probe dc measurement technique,[22] where a Keithley 2440 sourcemeter and a 2182A nanovoltmeter are used as current source and voltage detection instruments, respectively. The CPP MR-*H* loops were measured in fabricated pillarlike nanodevices for a dc current $I = 0.5$ mA, whereas the CIP MR-*H* ones were collected in rectangular, 2 mm × 8 mm, pieces of the as-grown SL for $I = 10$ mA, where **I**||**a** and the resistance was measured along **H** direction. The current polarity was kept unchanged for the whole set of MR measurements. The CIP MR-*H* curves were adequately corrected against the nonmagnetic contribution of the bottom Nb and Y layers, see Sec. III. The MR was calculated according to the following relationship: $\frac{\Delta R}{R_0} = \frac{R(H)-R_0}{R_0}$, where $R(H)$ is the sample resistance under an applied magnetic field and $R_0 = R_{H=0}$.

A Cu overlayer, ≈250-nm thick, was sputtered onto the as-grown (0001)Dy/Y superstructure, in order to prepare the Dy/Y SL for CPP-MR measurements. Subsequently, the sample was patterned by using standard optical lithographic and reactive ion etching techniques and, after that, by using a focused ion beam (FIB) microscope as a nanomilling tool, a number of pillarlike nanodevices were fabricated.[23,24] Figure 1 shows a sketch of the nanofabrication process and an FIB image of a typical pillarlike nanodevice. We experimentally find that the resistance measured in pillarlike constrictions is mainly contributed by *I* traveling transversal to the Dy-Y interfaces in the sculpted nanodevice. This can be calculated from the geometrical dimensions of the central track and pillarlike nanodevice[23] (see Fig. 1) and taking into account that the out-of-plane resistivity, measured in a pillarlike nanodevice, is a factor five larger than the in-plane one, see Sec. III.

The formation of a 2–3-nm-thick RE-oxide layer on the side walls of the RE-based multilayered nanodevice occurs immediately after exposing it to air and its long-term stability is given by the UHV conditions during the deposition of RE thin films,[25] so that, $P \leqslant 10^{-8}$ mbar leads to the formation of stable passive oxide layer.[26] MR measurements in the Dy/Y (Ref. 21) SL spaced out a few months in time and carried out in a same nanodevice are found reproducible (±3%), proving the long-term chemical stability of our RE-based nanodevices.

III. RESULTS AND ANALYSIS

A. X-ray diffraction characterization

A longitudinal on-axis scan of the wave-vector transfer, *Q*, in the Dy/Y SL shows sharp Bragg peaks for the sapphire

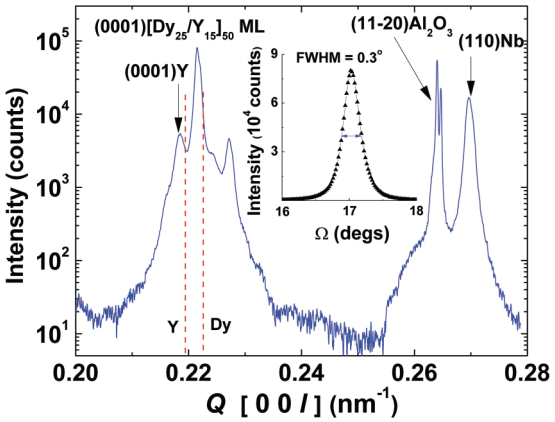

FIG. 2. (Color online) (a) X-ray diffraction intensity for a longitudinal scan of the wave-vector transfer, $\boldsymbol{Q}$, along [00l] direction in an SL with nominal structure $(Dy_{25}/Y_{15})_{50}$ showing Bragg reflections from the $(11\bar{2}0)Al_2O_3$ substrate, (110)Nb buffer and (0001)Y seed layers as well as those corresponding to the (0001)-oriented Dy/Y epitaxial superstructure. Dashed lines mark the (0001) and (110) Bragg reflections for Y and Dy, and Nb bulk metals, respectively. Insert graph is a transversal scan. For further details see text.

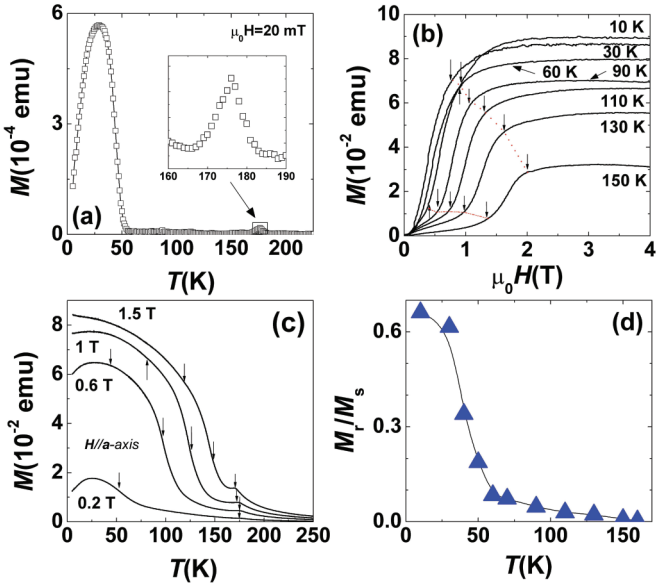

FIG. 3. (Color online) Zero-field-cooled (ZFC) magnetization M as a function of temperature T in a $[Dy_{26\pm1}/Y_{14\pm1}]_{50}$ SL. The insert graph shows a magnification of the cusplike feature at high T. (b) ZFC magnetization vs applied magnetic field **H**. The arrows indicate the critical fields at which a magnetic phase transition takes place. (c) ZFC magnetization curves vs T at selected H values. The arrows indicate the critical temperatures at which a phase transition occurs. (d) Ratio between remanent and saturation M, that is, M_r/M_s, as a function of T. In all cases, **H** is along the **a** axis of the hexagonal lattice.

reflection (110), $Q = 2.646$ Å^{-1}, Nb reflection (110), $Q = 2.680$ Å^{-1}, and a number of (002) reflections corresponding to the Y seed layer and to the Dy/Y multilayered structure, centered at $Q = 2.185$ and 2.215 Å^{-1}, respectively, as displayed in Fig. 2. This proves that the Dy/Y SL is crystallographically coherent along c direction. The full width at half maximum (FWHM) at the main Dy/Y SL reflection yields $\sim 0.3^\circ$, consistent with early data in Ho/Y (Ref. 27) ($\sim 0.2^\circ$) and Dy/Ho (Ref. 28) ($\sim 0.3^\circ$). From the longitudinal scan shown in Fig. 2, we calculate that the average Dy/Y bilayer thickness is $t \simeq 11$ nm and the structural coherence length $\xi \simeq 66$ nm.

The in-plane lattice mismatch between Y and Dy is $\sim -1.5\%$.[29,30] By using the model developed by Jehan *et al.*,[27] we calculate that the average thickness for Dy and Y layers is $t_{Dy} = 26$ MLs and $t_Y = 14$ MLs, respectively, the interplanar spacing for the Dy layers is $d_{Dy} = 2.8145$ Å, and the interdiffusion and/or roughness at the Dy-Y interface is $\lambda = \pm 1$ ML. We estimate from these that the strain transversal to the deposition plane is $\varepsilon_{out} = (d_{Dy} - d^b)/d^b = -4.6 \times 10^{-3}$, where $d^b = 2.8275$ Å is the interplanar spacing along c axis in bulk Dy. Making use of the Poisson's relationship in hexagonal symmetry,[31] $\varepsilon_{out} = -2\varepsilon_{in} c_{13}/c_{33}$, where ε_{in} is the strain in the basal plane (BP) and assuming that ε_{in} is isotropic and the elastic constants c_{ij} for the buried Dy layers are roughly similar to those in bulk Dy,[32] taking $c_{13} = 20.77$ GPa and $c_{33} = 78.9$ GPa, we estimate that $\varepsilon_{in} = 8.74 \times 10^{-3}$.

B. Magnetic characterization

The zero-field cooled (ZFC) M-T curve displayed in Fig. 3(a) shows two magnetic transitions in the Dy/Y SL. The small cusplike feature, which emerges in the high-temperature range, suggests the onset of a helical-antiferromagnetic (H-AFM) phase for temperatures below $T_N^{sl} \simeq 176$ K, which is very close to $T_N = 179$ K in bulk Dy.[33] A notably larger feature appears at lower temperatures, where as temperature rises, M gradually increases and peaks at $T = 30$ K. For $T > 30$ K, M steadily diminishes down to $T = 50$ K and becomes very small for higher temperatures. We interpret this nonmonotonic variation of M with temperature, alongside the absence of an abrupt and sharp drop in M at $T_C^{sl} \simeq 50$ K—notice that the drop in M spans over a 20 K temperature window—as a sign of the onset of a complex noncollinear magnetic structure in Dy/Y SL for $T < 50$ K.

The ferromagnetic (FM) phase transition in bulk Dy occurs at $T_C = 89$ K (Ref. 33) and this is accompanied by a spontaneous magnetoelastic (MEL) distortion of the BP.[34] The MEL strain favors the FM phase against the helical-AFM phase, becoming the driving force behind the first-order FM transition,[35] which suggests the alteration of FS topology by the MEL strains. Thus the shift in T_C^{sl} towards lower temperatures can be attributed to the combined effect of epitaxial clamping and tensile stress[36] exerted by the nonmagnetic Y layers on the Dy ones, which are opposed to the spontaneous MEL distortion,[34] and thus prevent to develop in full the MEL strains in Dy/Y SL, forcing the FM transition to occur at a lower temperature in Dy/Y (Refs. 37 and 38) than in Dy bulk.

Studies of the magnetization process in a spin-spiral magnetic structure[39,40] predicted the existence of three magnetic phases: a zero-field H-AFM, a fan, and an FM. ZFC M-H curves show a single magnetic phase transition for $T \leqslant 50$ K, whereas two transitions are observed for those obtained at $T > 50$ K, see Fig. 3(b). This indicates the onset of intermediate fan-type magnetic structures[41] in the Dy/Y SL, in analogy to bulk Dy. Additionally, M-H curves collected at $T < 50$ K display initial slopes far from reaching the demagnetization

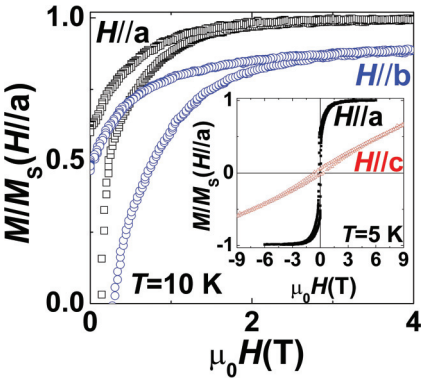

FIG. 4. (Color online) Half hysteresis loops, M-H, collected in the $[Dy_{26\pm1}/Y_{14\pm1}]_{50}$ superlattice at $T = 10$ K, for the applied magnetic field H along the hard (circles), $\mathbf{H}||\mathbf{b}$, and easy (squares), $\mathbf{H}||\mathbf{a}$, directions for the magnetization M, where $M_s^a = 2900$ emu/cm^3 and $M_s^b = 2555$ emu/cm^3 are the saturation M along $\mathbf{a}$ and $\mathbf{b}$ directions, respectively. Insert graph shows M-H loops collected at $T = 5$ K for H applied along $\mathbf{a}$ and $\mathbf{c}$ directions in the hexagonal lattice.

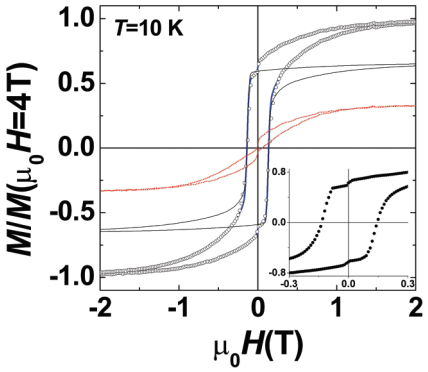

FIG. 5. (Color online) Hysteresis loops at $T = 10$ K by applying the magnetic field, $\mathbf{H}$, along $\mathbf{a}$ direction collected in (empty circles) $[Dy_{26\pm1}/Y_{14\pm1}]_{50}$ superlattice (SL) and (continuous black line) a Y/Dy/Y trilayer nanostructure. The dotted-red line represents the substraction of the above M-H loops. The insert graph is a magnification of the M-H loop. For further details see text.

limit, $1/N_d$, given by the demagnetization factor N_d in a FM material.[42] If we assume a fully coherent FM ordering below $T = 50$ K for the Dy blocks, given that $\mathbf{H}||\mathbf{a}$, $N_d \simeq 0$, and thus, M should show a sharp increase under a small increase in H, which is not observed. The absence of this feature suggests that the magnetic ordering at $T \leqslant 50$ K is other than a FM arrangement. Resembling the ZFC M-T curve at $\mu_0 H = 20$ mT, M-T curves collected at higher H also exhibit a nonmonotonous behavior, only suppressed for $H \geqslant 1$ T, as shown in Fig. 3(c).

A complete suppression of FM order was earlier reported on Dy/Y SLs.[37] In our Dy/Y SL, M_r/M_s ratios, where M_r and M_s are remanence and saturation magnetization, respectively, support the hypothesis of the onset of a complex noncollinear magnetic structure at $T < 50$ K other than a spin-spiral magnetic structure in the Dy/Y SL, see Fig. 3(d). Indeed, notice that the ratio $M_r/M_s = 0.6$ obtained at $T = 10$ K can be reproduced by a magnetic structure consisting of a noncollinear block-by-block arrangement with a modulation period of $4(t_{Dy} + t_Y)$, where M in adjacent FM Dy blocks is oriented along the nearest $\mathbf{a}$ directions.

The long-range periodic magnetic ordering found in RE-based[43] SLs is accomplished by means of an RKKY-type[44] coupling, where the sign of the interlayer exchange coupling depends in an oscillatory way on the thickness of the nonmagnetic layers. Thus the magnetization data shown in Fig. 3 are fully consistent with the onset of a staggered magnetic structure at $T < 50$ K, so that Dy moments located in layers within a same Dy block tend to order ferromagnetically, meanwhile those located in layers belonging to adjacent Dy blocks present a weak AFM coupling, forming a noncollinear magnetic arrangement. This is in line with a weak AFM ordering earlier found in Gd/Y (Ref. 45) SLs for $t_y = 14$ ML.

In analogy to helical structures found in Dy/Y (Ref. 37) and Ho/Y (Ref. 27) SLs, the spin-spiral magnetic structure developed in Dy/Y SL is expected to be largely coherent across several Dy-Y bilayers, including a phase shift of about 52° between the spin-spiral arrangements developed in consecutive Dy blocks. From prior neutron studies,[37,38] we deduce that the average turn angle ω for the helical arrangement in Dy/Y SL may vary between $\omega \approx 45°$ ($\mathbf{Q}_i = 0.25\mathbf{c}^*$) at T_N^{sl} down to $\omega \approx 32°$ ($\mathbf{Q}_i = 0.177\mathbf{c}^*$) right before $T = 50$ K, where $\mathbf{Q}_i$ is the intrablock modulation wave vector of the helixlike magnetic arrangement. Therefore, apart from the presence of interfaces, the spin-spiral magnetic structure in Dy/Y SL is essentially similar to that found in Dy bulk,[46] but ω is slightly shifted towards larger values in Dy/Y SL. However, differences arise when chemical and magnetic modulation are put together. Thus the discrete Fourier transform (DFT) of the expected spin-spiral magnetic structure in the Dy/Y SL at T_N^{sl}, not shown here, reveals the splitting of the fundamental harmonic, Q_i, into twine $Q_{-i} = 0.219\bar{c}^*$ and $Q_{+i} = 0.269\bar{c}^*$ *superlattice* structure harmonics halved in intensity, so that their spacing is $\Delta Q = Q_{+i} - Q_{-i} = 2\bar{c}^*/t$, where $t = t_{Dy} + t_y = 40$ MLs and $\bar{c}$ is the average c parameter in the Dy/Y SL.

M-H loops collected by applying $\mathbf{H}$ along the high-symmetry axes of the hexagonal lattice indicate that c plane is the easy plane for M and $\mathbf{a}$ direction is the easy one in the basal plane (BP) of the HCP structure in the Dy/Y SL, see Fig. 4(a). The c-plane anisotropy energy reads as[2] $E_k(\phi) = E_k^0 + K_6^6 \cos 6\phi$, so that the in-plane effective sixfold magnetic anisotropy constant K_6^6 can be determined by measuring M-H curves along the hard and easy directions for M in the c plane as follows:[47] $K_6^6 = [\int^{M_b} H_b(M)dM - \int^{M_a} H_a(M)dM]/(\cos 6\phi_b - \cos 6\phi_a)$, where $\phi_b = \pi/6$ and $\phi_a = 0$, see Fig. 4(b). At $T = 10$ K, we find that $K_6^6 = -1.21 \times 10^7$ erg/cm^3, decreasing down to $K_6^6 = -5.33 \times 10^6$ erg/cm^3 at $T = 50$ K, which means a twofold increase when compared to K_6^6 in bulk Dy,[48] consistent with the diminishing of K_6^6 under compression stress found in Ho/Lu (Ref. 49) SLs.

Importantly, a two-step magnetization reversal process, which constitutes a conclusive evidence of the coexistence of FM and weak AFM order in the Dy/Y SL, appears in the M-H loops collected at $T < 50$ K, as shown in Fig. 5, in contrast to hysteresis loops collected at $T > 50$ K, see Fig. 6. Modeling hysteresis[50] is a complex theme, so we have opted for an all-experimental approach to test whether M-H loops at $T < 50$ K can be reproduced by juxtaposing a FM-like M-H

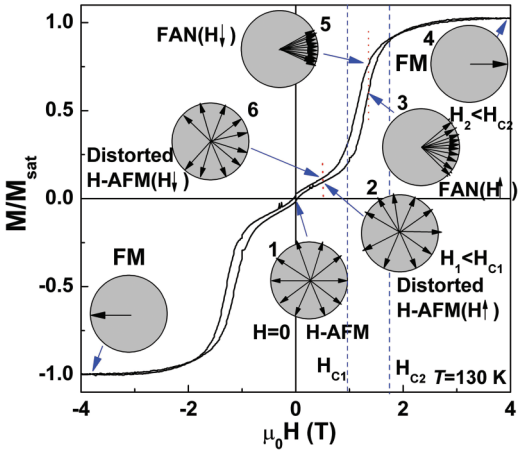

FIG. 6. (Color online) Hysteresis loop collected in a $[Dy_{26\pm1}/Y_{14\pm1}]_{50}$ superlattice at $T = 130$ K, where the applied magnetic field, **H**, is along the **a** axis of the hexagonal-close-packed structure. The schematic drawings represent the expected field-induced magnetic phases. For those labeled from 1 to 4, **H** strength rises, and they represent (1) helical-antiferromagnetic (H-AFM) phase, (2) distorted H-AFM state, (3) fan-type phase, and (4) ferromagnetic (FM) phase. For those drawings labeled as 5 and 6, **H** is reversing down to zero from high field. The arrows represent the orientation of the Dy magnetic moments in the basal plane (BP). Consecutive arrows indicate moments in adjacent BPs, which form a modulated magnetic structure when moving along the c axis. H_{c1} and H_{c2} are the critical fields for the first- and second-order magnetic phase transitions, respectively, marked by vertical dotted lines. The (↑) and (↓) arrows denote increasing and reversing **H**, respectively. For further details see text.

loop and a second one having AFM-like features. To that end, we collected M-H loops in a strainedlike c-grown Y/$Dy_{t'}$/Y trilayer,[38] where the Dy layer thickness is $t' = 280$ nm. The trilayer presents a spontaneous FM transition at $T_C \approx 50$ K and shows a slightly smaller coercivity, which is rescaled to match that of the Dy/Y SL. At $T = 10$ K, subtracting the M-H loop collected in Y/Dy/Y trilayer from that in Dy/Y SL results in an AFM-like[51] M-H loop, as seen in Fig. 5, where we find that $M_{Dy/Y}(H) = aM_{Y/Dy/Y}(H) + bM_{AFM}(H)$, so that $a = 0.64$ and $b = 0.36$. Therefore the FM-like loop represents the incoherent magnetization reversal process of the Dy layers, that is, Neél-type domain-wall (DW) nucleation and DW movement, whereas the AFM-like M-H loop represents the coherent rotation towards **H** of M in each Dy block.

Figure 6 illustrates the magnetization process in a simple c-plane spin-spiral magnetic structure,[39,41] given that K_6^6 decays rapidly with temperature.[48] Thus an in-plane H turns the zero-field H-AFM structure into a distorted helix, yielding a small M, which smoothly increases as H rises; as H is further increased, a first-order magnetic phase transition occurs at the critical field $H_{c1} = 0.97$ T, where the distorted H-AFM phase is turned into a fan magnetic structure, where M sharply increases with H. A second-order magnetic phase transition occurs at the critical field $H_{c2} = 1.85$ T, where the fan arrangement is turned into a fully aligned state along **H** direction.

The critical fields, H_c's, are obtained from the ZFC M-H and M-T curves displayed in Figs. 3(a) and 3(b). The criteria to obtain H_c consists of taking the intermediate point over

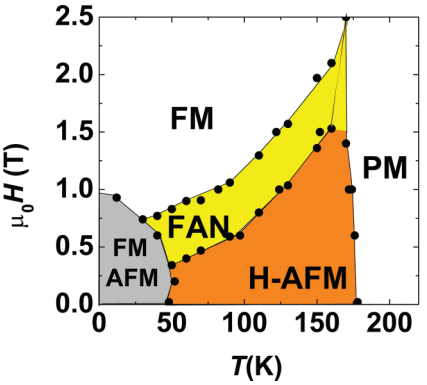

FIG. 7. (Color online) Magnetic phase diagram for the c-grown $[Dy_{26\pm1}/Y_{14\pm1}]_{50}$ superlattice so that the applied magnetic field **H** is along **a** direction. Five magnetic phases are identified: paramagnetic (PM), helix-antiferromagnetic (H-AFM), fan, ferromagnetic (FM), and complex FM + AFM. For further details see text.

the locus of points forming the elbowlike segment, which marks a slope change in M-H and M-T curves. By comparing the magnetic phase diagram (MPD) in the Dy/Y SL, see Fig. 7, to that in bulk Dy,[33,52–54] we highlight the following aspects. (1) The H_c's associated to the magnetic transitions from H-AFM into fan phase and fan phase into FM phase are shifted towards higher H values in the Dy/Y SL. (2) The magnetic transition from H-AFM into FM phase in bulk Dy is suppressed in the Dy/Y SL, where H-AFM and fan phases are stable over the same temperature range. (3) Finally, the zero-field FM transition is strictly confined to Dy layers belonging to the same block, where adjacent Dy blocks are antiferromagnetically coupled, forming a staggered noncollinear magnetic arrangement.

C. Magnetoelectric characterization

Figure 8(a) displays the c axis resistivity in the Dy/Y SL, ρ_c^{sl}, which shows the following aspects of interest. (1) The most important attribute in the ZFC ρ_c^{sl} is the absence of the bumplike feature observed in bulk Dy[55] around about T_N and the sharp

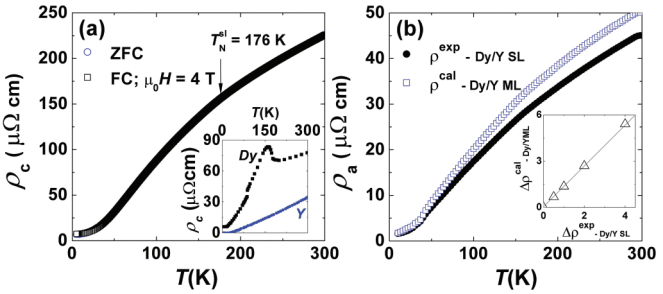

FIG. 8. (Color online) (a) Zero-field-cooled (ZFC), circles, and field-cooled (FC), squares, resistivity curves measured along the **c** axis of the hcp structure, ρ_c, on a pillarlike nanodevice fabricated in a $[Dy_{26\pm1}/Y_{14\pm1}]_{50}$ SL. The insert graph shows ZFC ρ_c-T curves for Dy[55] and Y[56] bulk. (b) ZFC in-plane resistivity ρ^{exp} measured in the Dy/Y SL for $\mathbf{H}\|\mathbf{I}\ \|\mathbf{a}$ axis (circles) and the calculated in-plane ρ^{cal} linked to the Dy/Y multilayer stack only (squares). The insert graph shows the conversion factor ζ where $\Delta\rho^{cal}$ is plotted against $\Delta\rho^{exp}$. For further details see text.

drop-off at T_C, see insert graph in Fig. 8(a); notice that ZFC and FC $\rho_c^{\rm sl}$-T curves barely deviate from each other. This points out that the GMR effect[12] is suppressed, which suggests a severe alteration of the superzone effect in the Dy/Y SL. (2) The ZFC $\rho_c^{\rm sl}$ is continuous through the Nb superconducting temperature, which denotes that $\rho_c^{\rm sl}$ is due to current flowing transversally to the Dy-Y interfaces in the nanodevice. (3) Making use of a simple block-model, $\rho_c^{\rm sl}$ should be mostly dominated by the high-resistive Dy[55] layers, given that the Y[56] ones present a lower resistivity. Assuming this, if we compare $\rho_c^{\rm sl}$ to the c -axis resistivity in bulk Dy, $\rho_c^{\rm Dy}$, we find that $\rho_c^{\rm sl}/\rho_c^{\rm Dy}$ amounts to $\approx$2.9 at $T = 300$ K, decreasing down to $\approx$1.3 at $T = 10$ K.

We speculate over the likely origin of the excess out-of-plane resistivity, which we attribute to an interface effect, due to the strong modulation of the ionic pseudopotential, $\approx Z$, where Z is the atomic number of the $Dy^{3+}(Z = 66)$ and $Y^{3+}(Z = 39)$ ions. Thus electrons traveling along c axis in the Dy/Y SL will encounter an abrupt steplike perturbation in the electrostatic scattering at the sharp Dy-Y interfaces. An early study showed[57] that the emergence of weakly localized states and charge transfer across interfaces originated in a band-matching misfit effect due to the chemical modulation explained the observed changes in the single-ion MEL parameters in Ho/Lu SLs. In analogy to this, we anticipate that the strong chemical modulation effect in Dy/Y SL is likely to be the source of the excess out-of-plane resistivity, where Dy-Y interfaces will act in this case as spin-independent scattering centers, in close resemblance to the excess resistivity due to impurity ions in a metallic matrix.[58,59]

In line with $\rho_c^{\rm sl}$, the in-plane resistivity $\rho_a^{\rm sl}$ shows a smooth slope change around about $T_N^{\rm sl}$, see Fig. 8(b), in contrast to the pronounced feature shown by its counterpart in bulk Dy.[55] We stress that, as a result of the deposition techniques,[21] the in-plane current is shunted by the low-resistive Nb[60] buffer and Y[56]-seed bottom layers and, therefore, the collected $\rho_a^{\rm sl}$ in the superstructure differs from the resistivity due to the Dy/Y ML, $\rho_a^{\rm ml}$. In order to calculate $\rho_a^{\rm ml}$, we have modeled $\rho_a^{\rm sl}$ according to a *multilayered parallel resistor* model,[61]

$$\frac{t_{\rm sl}}{\rho_a^{\rm sl}} = \frac{t_{\rm nb}}{\rho_{\rm nb}} + \frac{t_{\rm Y}}{\rho_{\rm Y}} + \frac{t_{\rm ml}}{\rho_a^{\rm ml}}, \tag{2}$$

where $\rho_{\rm nb}$ and $\rho_{\rm Y}$ are Nb[60] and Y[56] in-plane resistivity; $t_{\rm sl}$, $t_{\rm nb}$, $t_{\rm Y}$, and $t_{\rm ml}$ are the Dy/Y SL ($\sim$665 nm), Nb-buffer, Y-seed plus Y-capping layers ($\sim$50 nm), and the Dy/Y multilayer ($\sim$565 nm) thickness, respectively. We have also considered that $\rho_{\rm nb}$ and $\rho_{\rm Y}$ can be thickness dependent according to Fuchs-Sondheimer theory,[62–64] which reads

$$\rho(t) = \rho_b \left(1 + \frac{3}{8}\frac{L_e}{t}\right), \tag{3}$$

where ρ_b is the bulk resistivity, t is the thin-film thickness, and $L_e \sim 6$ nm[65,66] for Nb. Thus, from Eq. (3), we obtain $\rho_{\rm nb}(t_{\rm nb})$ and $\rho_{\rm Y}(t_{\rm Y})$ and inserting these latter in Eq. (2), we determine $\rho_a^{\rm ml}$, as shown in Fig. 8(b). We have also estimated a conversion factor ζ, which relates a change in $\rho_a^{\rm sl}$ to its counterpart in $\rho_a^{\rm ml}$ and we find $\zeta \sim 1.4$ for $\Delta\rho_a^{\rm ml}/\rho_{a,o}^{\rm ml} \leqslant 4\%$, see insert graph in Fig. 8(b). Importantly, ζ will be used to correct the in-plane MR curves. On the other hand, $\rho_a^{\rm ml}$ is almost half of its counterpart in bulk Dy,[55] as shown in Fig 8(b). This is consistent with our previous thesis, since now $\rho_a^{\rm ml}$ will be dominated by the low-resistive Y layers, where electrons flowing in-plane will be scattered before reaching the Dy-Y interface, given that the electron mean-free path L_e in both Dy and Y layers is $L_e \sim$ 1–2 nm,[61,67] and, therefore, $L_e < t_{\rm Dy}, t_y$.

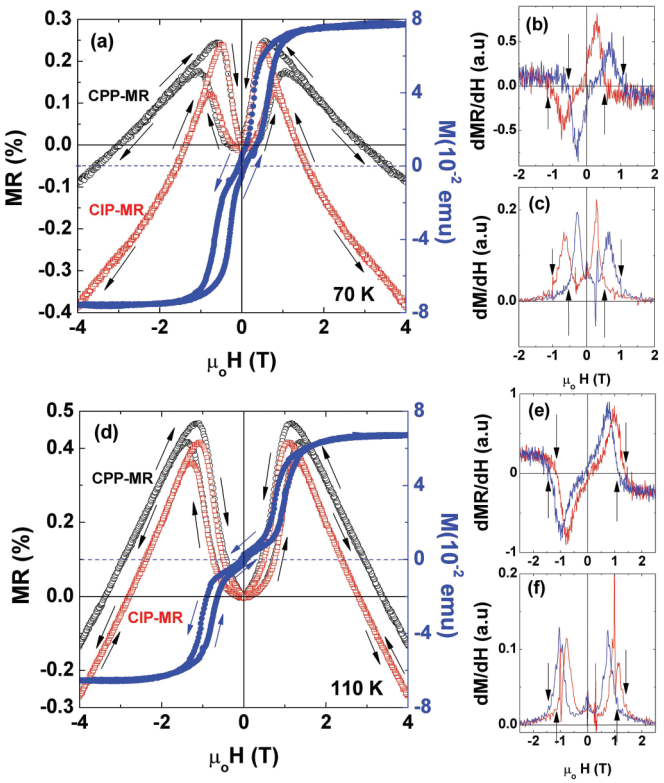

FIG. 9. (Color online) (Left) Current perpendicular to plane magnetoresistance (CPP-MR) and hysteresis loops at (a) $T = 70$ and (d) 110 K measured on a $[Dy_{26\pm1}/Y_{14\pm1}]_{50}$ SL. (Right) dMR/dH and dM/dH are the derivative functions of the CPP MR-H and M-H curves with respect to the applied magnetic field $\mathbf{H}$ obtained at 70 K (b) and (c) and 110 K (e) and (f), where $\mathbf{H}\|\mathbf{a}$ axis of the HCP structure, respectively. Crossings through zero in dMR/dH and slope changes in dM/dH are marked by arrows. For further details see text.

A thorough understanding of the changes introduced into the electrical resistivity in RE-based heterostructures, derived mostly from their low dimensionality, requires of performing *ab initio* electronic band structure calculations,[68] only recently applied to explore the FS in FM bulk RE metals.[69,70] Thus, it is well-known that the c/a ratio plays a significant part at determining the FS in bulk RE metals,[71,72] so that the resistivity of strained RE-based thin films is likely to depart substantially from that of bulk counterparts. However, this matter is beyond the scope of this study, and as far as we possibly can, we will discuss our results within the well-established EW[16] theory.

Let us now focus our attention on the magnetoresistance in the spin-spiral magnetic phase, the most relevant to noncollinear spintronics. As shown in Fig. 9, MR-H loops show in both geometries a similar nonmonotonic dependence on H, so that, MR ratios increase with H and present hysteresis for $H < H_{c2}$, whereas for $H > H_{c2}$, MR presents a linear (negative slope) and unsaturated variation with H, where MR ratios barely exceed -0.6% at the maximum applied field,

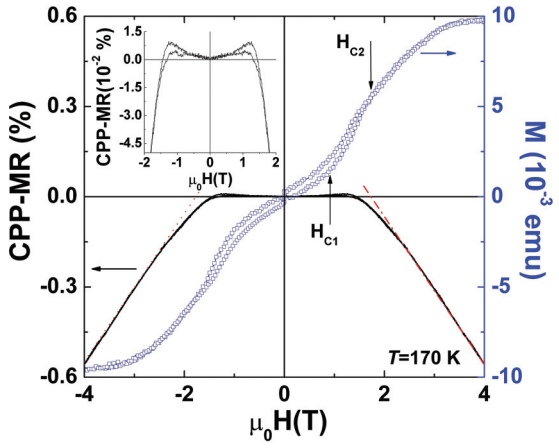

FIG. 10. (Color online) M-H and CPP MR-H loops collected in a $[Dy_{26\pm1}/Y_{14\pm1}]_{50}$ SL at $T = 170$ K. The applied magnetic field **H** is along the **a** direction of the HCP structure. H_{c1} and H_{c2} are marked by arrows. The insert shows a magnification of the MR-H loop. For further details see text.

4 T. MR-H and M-H loops are intimately related to each other, that is, MR follows the changes induced by H in the magnetic structure for $H < H_{c2}$. We observe that the MR ratios in both geometries increase as M does for increasing H and, *vice versa* for reversing H; more importantly, MR and M present the maximum slope (positive or negative) at the same H values. This aspect is clearly shown by $d\mathrm{MR}/dH$ and dM/dH curves, which both yield extremes for $H \simeq 0.7$ T(↑) and $H \simeq 0.3$ T(↓) at $T = 70$ K and for $H \simeq 0.97$ T(↑) and $H \simeq 0.77$ T(↓) at $T = 110$ K, where the up (↑) and down (↓) arrows denote increasing field from zero up to 4 T and reversing field down to zero from 4 T, respectively, see right-side panels in Fig. 9. In addition, we also observe that MR shows a trend change for $H = H_{c2}$ when M tends to saturation. This latter match is illustrated at $T = 70$ K, see Figs. 9(b) and 9(c), and at $T = 110$ K, see Figs. 9(e) and 9(f), where $d\mathrm{MR}/dH$ crosses through zero and dM/dH presents a slope change simultaneously for $H_{c2} \sim 1.05$ T(↑) ($T = 70$ K) and for $H_{c2} \sim 1.45$ T(↑) ($T = 110$ K).

As displayed in Fig. 10, at a temperature lower but very close to T_N^{sl}, the M-H loop already presents hysteresis and a slope change at low field H_{c1}, which indicates the onset of the fan phase. At H_{c2}, the M-H loop is closed, but for $H > H_{c2}$, M shows an unsaturated variation with H, forced magnetization. On the other hand, for $H < H_{c2}$, a closer look at CPP MR-H loop reveals hysteresis and a nonmonotonic variation with H and a positive but very small MR ratio, $\leqslant 10^{-2}\%$, see Fig. 10. Replicating the behavior shown at lower temperatures, CPP-MR shows a linear (negative slope) and unsaturated variation with H for $H > H_{c2}$, where typically MR $< -0.6\%$ at the maximum applied field.

As an aside, we notice that M-H loops collected in patterned[73,74] and as-grown samples usually show a shift in coercive and saturation fields. We experimentally observe a fine match-up between characteristic features in CPP MR-H and M-H loops, as shown in Fig. 9. This observation reflects on the fact that the strain in the Dy layers is determined by the interleave nonmagnetic Y ones[27] and, therefore, is basically unchanged by the nanofabrication process. However, a different scenario is found in bilayers,[73,74] where a typically thick buffer layer imposes the in-plane lattice parameter to the on top deposited, usually strained, thin overlayer. In this case, the epitaxial strain can be further relaxed as a result of a lateral nanostructuring process.

We highlight the key aspects of our analysis: (1) The increase in MR (positive) in both CPP and CIP geometries is intimately related to the onset of a field-induced distorted H-AFM and fan magnetic phases. (2) For increasing H, the maximum positive CPP-MR is attained at $H_{c2}(\uparrow)$. For reversing H, positive CPP-MR values peak right after turning back to a fan-type phase from a fully aligned state. (3) CPP- and CIP-MR show a tendency change at around about $H = H_{c2}$, where MR starts decreasing and shows a linear and unsaturated dependence on H, becoming eventually negative at high applied fields. As temperature rises and gets closer to T_N^{sl}, the nonmonotonic variation of MR with H for $H < H_{c2}$ vanishes in both geometries. By contrast, the linear and unsaturated variation shown by MR for $H > H_{c2}$ persists even at $T \approx T_N^{\mathrm{sl}}$.

It is of interest now to clarify the origin of the positive MR in RE metals. In nonmagnetic metals, positive MR is due to the Lorentz effect,[75] also called Lorentz MR (LMR); in $3d$-based[76] multilayers, positive MR typically $<0.1\%$ is found and its origin is attributed to the LMR. In order for this to happen, a minimum condition must be fulfilled:[77]

$$\omega_c \tau = B\sigma/n_e e \gg 1, \tag{4}$$

where ω_c is the cyclotron frequency, τ is the relaxation time, $B = H + 4\pi M$ is the magnetic induction, σ is the conductivity, n_e is the number of conduction electrons per unit volume, and e is the electron charge. In heavy RE metals, σ is typically $\sim 5 \times 10^9\ \Omega^{-1}\ \mathrm{m}^{-1}$ at 4.2 K and n_e is $\sim 1 \times 10^{-29}\ \mathrm{m}^{-3}$. From this, we calculate that Eq. (4) leads to $\omega_c \tau \approx 10^{-2}$ B. Therefore, despite $M \approx 10$ T in Dy (at $T = 0$ K), we find it is highly unlikely that LMR yields a tangible contribution in RE metals, in line with early observations.[20]

It becomes clear now that the MR in RE metals possesses two distinctive origins: Bragg scattering of the CEs by the magnetic lattice[10,16] and scattering of the CEs by spin waves[78,79] (SWs) or so-called magnon magnetoresistance (MMR). The former requires that a periodic magnetic structure sets in[10] and, therefore, based on evidence that links positive MR to the onset of field-induced magnetic structures, see Fig. 9, we attribute the increase in MR to a modification in the superzone effect originated in the magnetization process of the anisotropic spin-spiral magnet, prior to reaching a fully aligned magnetic state along **H** direction. However, as can be seen in Figs. 9 and 10, the experiment shows a positive MR, in disagreement with the spin-disorder[17] model, see Eq. (1). This points to a needed reformulation of the spin-dependent scattering mechanism in RE metals, which should include spin correlations.[80]

In the high-temperature limit, that is, for $T \lesssim T_N^{\mathrm{sl}}$, the superzone contribution to the MR is almost negligible, as shown in Fig. 10. This fact allows us to explore the origin of the linear MR in the high-field limit free of interference. Thus, for $H < H_{c2}$, we have seen that MR changes very little with H and only when $H > H_{c2}$, this yields a linear (negative slope) and unsaturated dependence on H, which constitutes a fingerprint

of MMR[81] in highly anisotropic ferromagnets. In bulk Dy,[48] the dominant magnetic anisotropy K_2 varies from 5.5×10^8 erg/cm^3 at 0 K down to $\approx 5 \times 10^7$ erg/cm^3 at $T = 170$ K. From the latter, we calculate that $H_k = 2K_2/M_s \approx 12$ T, using $M_s \approx 850$ emu/cm^3. In highly anisotropic materials, Mihai *et al.*[81] demonstrated that as long as $H/H_k < 1$, which is the case in the Dy/Y SL, MR $\approx -CH$, where C is a T-dependent constant. As shown in Figs. 9 and 10, MR-H curves consistently show a linear (negative slope) scaling with H in the magnetized state, that is, for $H > H_{c2}$, in line to Mihai *et al.* findings, which strongly suggests that the origin of the high-field MR is due to the scattering of the CEs by magnons.

SW dynamics in Dy/Y MLs was recently investigated by Haraldsen*et al.*,[82] who found that the dispersion relation signature of the bulk Dy is essentially preserved, despite some differences associated to the ML superstructure. The SW dispersion relation in the presence of a magnetic field, $\varepsilon(k, H)$, and in the long-wavelength limit, takes the form[83]

$$\varepsilon(k, H_i) = g\mu_B H_i + \varepsilon(k), \tag{5}$$

where H_i is the internal magnetic field. The first term, $g\mu_B H \ll \varepsilon(k)$, in Eq. (5) represents an energy gap in the magnon spectrum arising from an effective H_i, so that $H_i = H - N_d M_s$. In our case, H is applied in-plane, which means that $N_d = 0$ and, hence, $H_i = H$. On the other hand, $\varepsilon(k)$ accounts for the SW energy-dispersion in zero field, which is given by the exchange stiffness constants and anisotropy energies.[84] In ferromagnetic RE metals,[85] if **H** is applied along the hard direction for M, $\varepsilon(k, H)$ varies smoothly with H for $H < H_c$, where H_c is the critical field for the induced FM transition, and increases linearly with H only for $H > H_c$. The above is the most likely situation to happen when **H** is applied along the easy direction in the spin-spiral magnetic phase, if we identify $H_c = H_{c2}$. In this way, at a given temperature, increasing H will enhance the SW energy gap in Dy/Y SL and, as a result, the magnon population, given by the Boltzmann distribution $\langle n_k(H) \rangle = [\exp(-\varepsilon(k, H)/k_B T) - 1]^{-1}$, will be diminished. Given that the probability of the magnon-electron spin-flip scattering is proportional to $\sum_k \langle n_k(H) \rangle$, the observed linear (negative slope) MR for $H > H_{c2}$ can be accounted for by the enhancement of the mean-free path in the magnetized state, derived from the increasing extrinsic SW energy gap with H, which limits the population of magnon modes at lower wave vectors.

EW[16] theory predicts that the resistivity transversal to the c axis, i.e., parallel to the new superzone boundaries, is of second order when compared to that determined along c axis. By extending this argument over MR(H), it is obtained that CPP-MR $\gg$ CIP-MR. However, the experiment shows a rather different picture, where CPP- and CIP-MR, associated to the maximum increase in MR, not only attain comparable values as shown in Fig. 11, but also the low-field MR (positive) attains similar values—in absolute terms—to that of the high-field limit MR (negative), see Fig. 9. The former reflects on the nonsphericity[70] of the FS in RE metals and the latter indicates that positive MR cannot be considered as an anomaly.[54] Additionally, CPP- and CIP-MR exhibit a similar

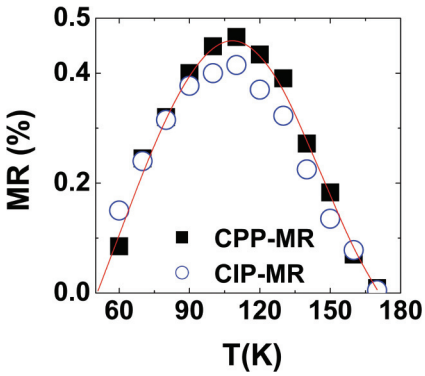

FIG. 11. (Color online) Temperature dependence of the maximum CPP-MR and CIP-MR attained by the onset of fan-type phases prior to the ferromagnetic phase transition. The applied magnetic field **H** is such as **H**||**a** axis in the $[Dy_{26\pm1}/Y_{14\pm1}]_{50}$ SL. The line is a fit according to the law, MR $= \delta_u/(1 - \delta_u)$. For further details see text.

nonmonotonic temperature scaling, given a pronounced peak at $T = 110$ K, which amounts to ~0.42%–0.47%.

Ab initio investigations[68] provide an accurate picture of MR sources in strongly correlated electron systems.[18] In particular, Antonov *et al.*[68] found two basic MR mechanisms, which are equally applicable to RE-based systems: (1) The occurrence of superzone band gaps, which disconnect FS sheets and, therefore, reduce the total FS area, leads essentially to an *isotropic magnetoresistance* and (2) *reshaping* or *deformation* of the FS sheets, unambiguously, leads to an *anisotropic magnetoresistance*. In the light of the isotropic MR in the Dy/Y SL, we can conclude that this is mainly due to the emergence of superzone band gaps.

IV. POSITIVE MAGNETORESISTANCE IN HELICAL MAGNETS

The emergence of noncollinear magnetic phases in RE metals reflects on a complex indirect-exchange[86] interaction. Making use of a simple three-plane coupling model,[87] ω in a simple spin-spiral-like magnetic structure is given by

$$\cos\omega = -J_1/4J_2, \tag{6}$$

where $\omega = Qc/2$ and $J_1 > 0$ and $J_2 < 0$ are the exchange parameters between nearest neighbors and next-nearest neighbors, respectively. As temperature decreases, K_6^6 increases rapidly, given rise to a *bunching*[46,88,89] effect of the magnetic moments along the easy directions. An in-plane applied H breaks the cylindrical symmetry of the anisotropic spin-spiral magnetic structure,[80] but neither the bunching effect nor the periodic magnetic structure are completely suppressed until a magnetized state is reached[90] for $H > H_{c2}$. It was originally proposed by Cooper *et al.*,[91] that as H increases and the uneven spatial distribution of the magnetic moments becomes more pronounced, the Fourier spectrum of the field-induced magnetic phases is increasingly populated by a large number of higher harmonics, $A_Q = \{s\mathbf{Q}\}_s$, where s is an integer number.

Here, we will explore in further detail the above argument. The free-energy F for the anisotropic spin-spiral magnetic

structure, including the Zeeman energy, reads as[80]

$$F = -\frac{1}{2}\sum_{i,j} J^2 \mathcal{J}_{ij}\cos(\phi_i - \phi_j) + \sum_i K_6^6 \cos 6\phi_i - \sum_i g\mu_0 J H \cos\phi_i, \tag{7}$$

where $\mathcal{J}_{ij}$ is the exchange parameter among $\mathbf{J}_i$ and $\mathbf{J}_j$ magnetic moments and we have assumed $|\mathbf{J}_i| = |\mathbf{J}_j| \equiv J$ and only considered the ϕ_i-dependent contribution to F. Now, the presence of the hexagonal anisotropy and Zeeman terms will distort the simple spin-spiral arrangement, where $\omega = \phi_i - \phi_j$ is given in Eq. (6). In order to find ϕ_i's that minimize F, we take $\partial F/\partial\phi_i = 0$, which yields

$$\sum_j J^2 \mathcal{J}_{ij}\sin(\phi_i - \phi_j) - 6K_6^6 \sin 6\phi_i + g\mu_0 J H \sin\phi_i = 0. \tag{8}$$

Firstly, we will consider the case in zero field, and we introduce the expansion $\phi_i = u_i + \gamma_k \sin 6u_i + \cdots$, in order to solve[92] Eq. (8), where $u_i = \mathbf{Q}\cdot\mathbf{R}_i$ and $\mathbf{R}_i$ is the position of the ith ion, then to first order in γ_K, solving Eq. (8) yields

$$\gamma_k = \frac{12K_6^6}{J^2[2\mathcal{J}(Q) - \mathcal{J}(5Q) - \mathcal{J}(7Q)]}, \tag{9}$$

where $\mathcal{J}(\mathbf{Q}) = \sum_j \mathcal{J}_{ij}\exp(-i\mathbf{Q}\mathbf{R}_j)$ is the Fourier transform of $\mathcal{J}_{ij}$. We obtain that the free energy per ion F/N, where N is the total number of RE ions, reads as

$$F/N = -\frac{J^2}{2}\left\{\mathcal{J}(Q) - \frac{\gamma_k^2}{4}[2\mathcal{J}(Q) - \mathcal{J}(5Q) - \mathcal{J}(7Q)]\right\}. \tag{10}$$

It is apparent from Eq. (10) that F is reduced proportionally to γ_k^2. This shows that the presence of hexagonal anisotropy introduces *twine* harmonics in the helical magnetic structure at wave vectors $5\mathbf{Q}$ and $7\mathbf{Q}$, *bunching* effect, and in higher order, at wave vectors $m6\mathbf{Q} \pm \mathbf{Q}$, where m is an integer number, so that, $m > 1$. For simplicity, we thereafter refer to them as $s_0\mathbf{Q}$.

Let us now consider an isotropic helical structure and the distortion caused by an in-plane applied magnetic field. Introducing the expansion $\phi_i = u_i + \gamma_h \sin u_i + \cdots$ and proceeding in the same way as above, to leading order in γ_h, solving Eq. (8) leads to

$$\gamma_h = \frac{2g\mu_B H}{J[2\mathcal{J}(Q) - \mathcal{J}(0) - \mathcal{J}(2Q)]}, \tag{11}$$

and substituting in Eq. (7), we obtain that

$$F/N = -\frac{J^2}{2}\left\{\mathcal{J}(Q) - \frac{\gamma_h^2}{4}[2\mathcal{J}(Q) - \mathcal{J}(0) - \mathcal{J}(2Q)]\right\}, \tag{12}$$

where F/N is reduced proportionally to γ_h^2. This means that in the low-field limit, the Zeeman term distorts the isotropic spin-spiral arrangement, introducing harmonics at wave vectors $2\mathbf{Q}$ and $\mathbf{Q} = 0$ (FM component). As H increases during the magnetization process of the helical structure, the Fourier spectrum of the field-induced magnetic phases will be populated by an increasing number of high-order harmonics at wave vectors $m\mathbf{Q} \pm \mathbf{Q}$. These will appear in F as terms of mth order in γ_h^2.

In a general case, i.e., $K_6^6 \neq 0$, finding an analytical solution to Eq. (8) is a complex matter. However, in analogy to the isotropic case, we find that the field-induced symmetry breaking of the pseudocylindrical arrangement presented by the anisotropic spin-spiral magnetic phase will cause, in the low-field limit, the appearance in the Fourier spectrum of additional harmonics, of unequal magnitude, at wave vectors $p\mathbf{Q}$, where $p = 0,2,4,6$, and 8, which will be added up to the existing ones in zero field. Furthermore, as H rises and the H-AFM phase is turned into a fan phase, the Fourier spectrum will be increasingly populated with higher harmonics at wave vectors $m(p\mathbf{Q}) \pm \mathbf{Q}$. In short, we thereafter refer to them as $s\mathbf{Q}$. Our analysis establishes that, just in the low-field limit, the number of harmonics that will appear in the Fourier spectrum of field-induced magnetic phases in a spin-spiral magnet undergoes a *threefold* increase when compared to that in zero-field magnetic phases. Furthermore, as H increases, the content in higher harmonics in the Fourier spectrum will be steadily enhanced, until reaching a fully magnetized state for $H > H_{c2}$.

Unfortunately, there exists a chronic lack of systematic neutron studies under applied magnetic field in helical RE-based systems and, as a result, little is known experimentally about the proposed enrichment of the Fourier spectrum in field-induced magnetic structures in helical magnets, apart from the decrease in $\mathbf{Q}$ upon transforming a spin-spiral into a fan-type magnetic phase.[93,94]

According to the EW model,[16] the magnetic contribution to the resistivity determined along c axis can be written as

$$\frac{\Delta\rho_{zz}}{\rho_{zz}^0} = \frac{\delta}{1-\delta}, \tag{13}$$

where ρ_{zz}^0 is the nonmagnetic contribution to the resistivity and δ accounts for the superzone contribution to the resistivity. Superzone band gaps Δ occur when $\mathbf{Q}+\mathbf{g}$ connects a degenerate pair of band states, where $\mathbf{g}$ is any reciprocal-lattice vector. For an in-plane spin-spiral RE metal, these gaps read as[95]

$$\Delta = 2M' S j_{f,sd}(\mathbf{Q}+\mathbf{g})|F_s(\mathbf{g})|, \tag{14}$$

where M' is a temperature-dependent factor associated with M, S is the $4f$ spin moment, $j_{f,sd}$ is the direct-exchange coupling between localized $4f$ and conduction $5d$-$6s$ electron densities, and $F_s(\mathbf{g})$ is the structure factor, which reads as

$$F_s(\mathbf{g}) = \frac{1}{z}\sum_{i=1}^{p}\exp(i\mathbf{R}_i\cdot\mathbf{g}) \tag{15}$$

summed over z atomic sites in an unit lattice cell in real space. The arising of $F_s(\mathbf{g})$ causes the mixing and associated band gaps to vanish for certain values of $\mathbf{g}$, which in turn entails dramatic consequences in multilayered heterostructures, as it will be shown later on. Now, according to EW theory,[16] δ primarily depends on Δ and the position of the Fermi surface relative to the new (magnetic) superzone boundary, Q. In order to consider the dependence of δ on H, the set of zero-field superzone boundaries, that is, $A_Q(H=0) = \{s_0 Q\}_{s_0}$ will be replaced by the set of field-dependent superzone boundaries,

$A_Q(H \neq 0) = \{sQ\}_s$, where we suppose that each harmonic that appears in the Fourier spectrum gives rise to a superzone boundary, for the sake of simplicity. According to EW theory,[16] three possible types of boundaries are found: (i) A first set of superzone boundaries $A_Q^{\mathrm{I}} = \{s_1 Q\}_{s_1}$ cuts the FS into two parts. Then, δ reads as

$$\delta_I = \frac{3\pi}{4} \sum_{s_1} \frac{s_1 Q}{k_{Fz}} \frac{\Delta}{E_F}. \tag{16}$$

(ii) A second set of superzone boundaries $A_Q^{\mathrm{II}} = \{s_2 Q\}_{s_2}$ touches the FS and possesses no second part, so that

$$\delta_{\mathrm{II}} = 1 - \sum_{s_2} \left[\left(\frac{s_2 Q}{k_{Fz}} \right)^3 + \frac{3\pi}{8} \frac{s_2 Q}{k_{Fz}} \frac{\Delta}{E_F} \right]. \tag{17}$$

(iii) Finally, a third set of superzone boundaries $A_Q^{\mathrm{III}} = \{s_3 Q\}_{s_3}$ does not reach the FS but this is distorted. We calculate that this condition leads to

$$\delta_{\mathrm{III}} \sim -\sum_{s_3} \left[\left(\frac{s_3 Q}{k_{Fz}} \right)^3 + \frac{k_{Fz}}{s_3 Q} \left(\frac{\Delta}{E_F} \right)^2 \right], \tag{18}$$

where E_F is the Fermi level, k_{Fz} is the projection of the Fermi vector k_F onto k_z, and s_1, s_2, and s_3 are integer numbers, summed over the relevant boundaries in each case, so that, $A_Q = A_Q^{\mathrm{I}} + A_Q^{\mathrm{II}} + A_Q^{\mathrm{III}}$. In general, δ in Eq. (13) will be contributed by all three types of superzone boundaries, so that

$$\delta = \delta_{\mathrm{I}} + \delta_{\mathrm{II}} + \delta_{\mathrm{III}}. \tag{19}$$

From Eqs. (16)–(19), it becomes clear that δ increases as H increases and A_Q gets increasingly populated, which in turn will be translated into a rise in resistance according to Eq. (13), in agreement with experiment, see Fig. 9. This also explains the rapid increase in MR with H observed in a fan phase, as shown in Fig. 9, given that this magnetic structure yields a complex Fourier spectrum, increasingly enriched as H rises. In addition, Eqs. (16)–(18) predict a faster change in δ with H, that is, with the increasing number of field-dependent superzone boundaries, if these latter are mainly of type I and/or II, that is, superzone band gaps. We find this in agreement with the isotropic character exhibited by the MR ratios, see Fig. 11, and with Antonov *et al.*[68] predictions.

In analogy to the established link between positive MR in spin-spiral structures and the increasing complexity of the field-induced magnetic phases, there are strong evidence that relate the onset of a complex magnetic structure to the emergence of a larger number of superzone band gaps. This is, for instance, the case in Tm,[96] which orders as a squarelike spin wave, in comparison to the spin-spiral spin wave developed in Ho.[88,89] Ultimately, the heavier populated Fourier spectrum in Tm is translated into a larger MR ratio in the former, ~80%,[13] than in the latter ~40%,[20] which offsets the fact that the leading band gap[95] in Tm is a fraction of that in Ho.

The dependence of the c-axis MR on temperature is given by Eq. (13), so that[16]

$$\delta_c = \Gamma_c \frac{\Delta}{\Delta_0}. \tag{20}$$

If we assume δ_c is mostly contributed by superzone boundaries type I and II, then $\Gamma_c \sim \sum_{s_1,s_2} \frac{(s_1+s_2)Q}{k_{Fz}}$ is introduced as an effective parameter determined by the sum over all contributions linear in the superzone band gaps in Eq. (19) and normally considered to be a constant[16] for the uth resistivity component. If we replace the energy-gap ratio in Eq. (20) by the ratio between the amplitudes, M_1/M_1^0, associated to the fundamental harmonic Q, see Eq. (14), then we obtain

$$\delta_c = \Gamma_c^\star\left(k_{Fz}^{-1}\right) Q(T) \frac{M_1}{M_1^0}. \tag{21}$$

A linear dependence for $Q(T)$ is a good approximation, see Sec. III B, and taking $\frac{M_1}{M_1^0} \approx m(T)$, where m is the reduced magnetization, we observe that Eq. (13) does not account satisfactory for MR(T) unless $\Gamma_c^\star$ is allowed to be a T-dependent function.[14] As shown in Fig. 11, the best fit is empirically achieved by using a second-order polynomial function $\Gamma_c^\star = \Gamma_c^{\star,\max} + \alpha(T - T_{\max}) + \beta(T - T_{\max})^2$, where $T_{\max} = 110$ K and the best-fit parameter are $\Gamma_u^{\star,\max} = 0.226\bar{c}$, $\alpha = 1.2 \times 10^{-4}\bar{c}$ K^{-1}, and $\beta = 6.2 \times 10^{-5}\bar{c}$ K^{-2}, where $\bar{c}$ is the average c lattice parameter in the Dy/Y SL. Two intimately related effects contribute to the T-dependent $\Gamma_c^\star$: (1) The FS topology in RE metals depends in a complex way on the c/a ratio,[72,97] which in turn varies with temperature[37,98] in a nonmonotonic manner, and (2) the sum over s_1 and s_2 in $\Gamma_c^\star$ depends on k_{Fz}, see (1), and on the interplay between sixfold magnetic anisotropy and exchange energies, which determine the Fourier spectrum of the zero-field spin-spiral magnetic structure, as earlier discussed. To end this discussion, we highlight that according to the model, the variation of the MR with temperature, as shown in Fig. 11, is mainly due to $\Gamma_c^\star$, since both Q and m present a smoother T dependence, where the size of Δ establishes how quickly $\Gamma_c^\star$ responds to changes in k_{Fz}.

V. SUPERZONES EFFECT IN MULTILAYERED NANOSTRUCTURES

Here we discuss the effect that the finite-size and chemical modulation may have upon the complexity of field-induced modulated magnetic structures in the Dy/Y SL and, by extension, in its magnetotransport properties.

A. Absence of the field-induced suppression of the superzones effect

We highlight that the DFT of the field-induced FM phase still produces a heavily populated spectrum, see Fig. 12, which shows harmonics at wave vectors $Q = 2m/t$, where $t = 40$ MLs and m is an integer number. The DFT associated to a collinear AFM phase possesses harmonics at $Q = Q_0 + 2m/t$, where the fundamental harmonic is $Q_0 = 1/2t$. Importantly, in this particular case, the third and fourth harmonics associated to the FM arrangement arise close to the harmonics $Q_{\pm i} \approx 0.22c^*$–$0.27c^*$ associated to the modulated spin-spiral magnetic structure developed in the Dy/Y SL, see Sec. III B. From Sec. IV, if A_Q remains heavily populated at high field, the MR ratio should yield a positive value. Recalling that the linear (negative slope) and unsaturated variation with H is due to the MMR, we attribute the absence

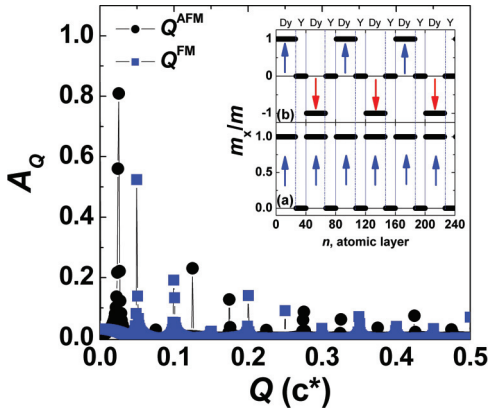

FIG. 12. (Color online) Fourier spectrum for a collinear antiferromagnetic (AFM), black circles, and ferromagnetic (FM), blue squares, magnetic structure developed in a $[Dy_{26\pm1}/Y_{14\pm1}]_{50}$ SL, where $Q_0 = Q_i/\pi = 0.125$ ML^{-1} and $Q_\pm = Q_0 \pm t^{-1}$, where $t = t_{Dy} + t_Y = 40$ monolayers (MLs). The Fourier frequency Q/π, is given in units of Λ^{-1}, where Λ is the period of the magnetic structure in MLs. The insert drawing is a sketch of a antiparallel ($H = 0$) and parallel ($H > H_k$) magnetic arrangement in Dy/Y SL, where $t_{Dy} = 26$ MLs and $t_Y = 14$ MLs are Dy and Y blocks thickness, respectively. See text for further details.

of a sharp drop-off in MR-H curves for $H > H_{c2}$ to the chemical modulation effect, which prevents a full suppression of superzone effect. This proves that a complete field-induced annihilation of the superzone effect may not occur as such in RE-based multilayered heterostructures, in clear contrast to bulk RE metals.

B. Finite-size effect contributes to enhance positive MR in RE-based nanostructures

We find that the low dimensionality of the Dy layers in the Dy/Y SL has two major effects. (1) Because of the epitaxial tensile stress, the in-plane sixfold magnetic anisotropy is enhanced in the Dy/Y SL when compared to bulk Dy, see Sec. III B. As shown in Sec. IV, an anisotropic spin-spiral arrangement possesses a heavier populated Fourier spectrum than its isotropic counterpart. Moreover, the larger K_6^6, the higher the intensity of the superzone boundaries originated in the *bunching* effect, note that $\gamma_k \sim K_6^6$, which in turn, leads to a larger positive MR in an anisotropic helixlike magnetic structure, although harder to magnetize. (2) Because of the long range of the RKKY coupling, finite-size effects are stronger in helical RE-based[99] systems than in collinear 3d-based nanostructures. In this context, the symmetry breaking of the the RKKY interaction by the chemical modulation is predicted to introduce major spatial alterations in the fan-type magnetic structures in layers at and near the interfaces.[100] Ultimately, this will reflect on a more complex Fourier spectrum for such spatially nonuniform modulated magnetic phases. Regardless, this matter may need further experimental work, here we anticipate that the tensile stress in the Dy layers and the presence of interfaces are effects that cooperate to produce a more complex Fourier spectrum in the Dy/Y SL than in bulk Dy. This additional complexity of the modulated magnetic structures explains the emergence of relatively larger positive MR ratios in Dy/Y SL when compared to the small bumplike (positive) features that appear in MR-H curves in strainfree bulk Dy.[20,54]

C. Suppression of the giant MR in multilayered heterostructures

We find that the negative MR in bulk Dy,[12,54] which is due to the annihilation of the superzone band gaps, is not strictly comparable with the positive MR ratios in the Dy/Y SL, which stems from the enhancement in the number of band gaps. However, it is equally apparent from Fig. 8 that the GMR effect is suppressed in the Dy/Y SL. Here, we discuss in some detail the likely sources for such a dramatic reduction.

(1) The first, more obvious, factor to consider is the excess resistivity linked to the spin-independent scattering contributions, see Fig. 8. Thus, at $T \gtrsim T_N$, the ratio $\rho_c^{sl}/\rho_c^{Dy} \approx 2$, which suggests that the spin-independent contributions to the resistivity in Dy/Y are twofold. Assuming the spin-dependent contributions unchanged, the CPP-MR ratios should be halved in the Dy/Y. This shows that spin-independent contributions to ρ_c^{sl} cannot explain by themselves alone the dramatic reduction in MR, which amounts to a downsizing factor of ≈35 for CPP-MR when we compare maximum MR ratios in absolute terms between the Dy/Y SL and bulk Dy.

(2) Another factor to consider would be a change in the direct coupling between 4f and 5d6s electron clouds, $j_{f,sd}$, due to changes in the interatomic distances and/or electronic band structure in the SL, see Eq. (14). Making use of the RKKY theory, T_C in RE metals can be written as[101]

$$T_C \propto S(S+1) j_{f,sd}^2 D(E_F), \tag{22}$$

where S is the localized spin and $D(E_F)$ is the density of states at the Fermi level. If we take $D(E_F) = 1.8$ states/eV per ion[102–104] for heavy RE metals, so that, in first order of approximation, $D(E_F)$ is assumed strain independent and, therefore, unchanged in layered Dy. Now, taking $j_{f,sd} = 0.088$ eV (Ref. 95) for bulk Dy and $T_C/T_C^{sl} = 1.78$, from Eq. (22), we calculate that the direct-exchange coupling between 4f and 5d6s electrons in Dy/Y SL is $j_{f,sd}^{sl} = 0.066$ eV. This predicts a downsizing factors of about 1.33, which again is not enough to fully justify the experiment.

(3) Finally, we will explore the consequences that the tetragonal-like enlargement of the unit lattice cell in the Dy/Y SL has upon $F_s(\mathbf{g})$. Thus, assuming Cartesian axes $\hat{\mathbf{x}}\|\mathbf{a}$, $\hat{\mathbf{y}}\|\mathbf{b}$, and $\hat{\mathbf{z}}\|\mathbf{c}$, where $\mathbf{a}$, $\mathbf{b}$, and $\mathbf{c}$ are the vectors of the ($\mathbf{a}$,2$\mathbf{b}$,$\mathbf{c}$) hcp unit lattice cell in bulk Dy, which has four atomic sites located at (0,0,0), $(\frac{1}{2},\frac{1}{2},0)$, $(\frac{1}{2},\frac{1}{6},\frac{1}{2})$, and $(0,\frac{2}{3},\frac{1}{2})$. We calculate that the structure factor in bulk Dy, F_s^{Dy}, can be written as

$$F_s^{Dy} = \frac{1 + e^{i(h+k)\pi} + e^{\frac{i}{3}(2h+k+3l)\pi} + e^{\frac{i}{3}(4k+3l)\pi}}{4}, \tag{23}$$

where (h,k,l) are integer numbers, so that $\mathbf{g} = h\mathbf{b}_1 + k\mathbf{b}_2 + l\mathbf{b}_3$ and ($\mathbf{b}_1$,$\mathbf{b}_2$,$\mathbf{b}_3$) are the vectors of the unit reciprocal lattice. In the Dy/Y SL, $\mathbf{a}$, $\mathbf{b}$, and $\mathbf{c}^{sl}$ are the vectors of the ($\mathbf{a}$,2$\mathbf{b}$,$\mathbf{c}^{sl}$) unit superlattice cell, so that $c^{sl} = 13c^{Dy} + 7c^{Y}$, where c^{Dy} and c^{Y} are the c lattice parameters for the Dy and Y layers,

respectively. The *superlattice* unit cell has 80 atomic sites with coordinates (0,0,n), $(\frac{1}{2},\frac{1}{2},n)$, $(\frac{1}{2},\frac{1}{6},\frac{n+1}{2})$, and $(0,\frac{2}{3},\frac{n+1}{2})$, where $n = 0,1,2,\ldots,19$. A *superlattice* reciprocal vector has the form $\mathbf{g}^{\mathrm{sl}} = h\mathbf{b}_1 + k\mathbf{b}_2 + l\mathbf{b}_3^{\mathrm{sl}}$ and the structure factor in the Dy/Y SL, F_s^{sl}, is immediate to obtain from Eq. (15). Our calculation shows that $F_s^{\mathrm{sl}} \neq 0$ if $h + k + l$ is odd, with l odd, and $F_s^{\mathrm{sl}} = 0$ otherwise. We find an expression for F_s^{sl}, which reads as

$$F_s^{\mathrm{sl}}(\mathbf{g}^{\mathrm{sl}}) = \frac{e^{i\frac{19l\pi}{20}}}{20} A_l \left(B_l + 2\cos\frac{l\pi}{2} \right), \tag{24}$$

where the coefficients $A_l = \sum_{r=0}^{r=4} \cos\frac{(2r+1)l\pi}{20}$ and $B_l = \sum_{r'=0}^{r'=1}[(-1)^{\frac{2}{3}} \cos\frac{(8+r')l\pi}{20} + (-1)^{\frac{1}{6}} \sin\frac{(8+r')l\pi}{20}]$. We observe that $F_s^{\mathrm{sl}}(\mathbf{g}^{\mathrm{sl}}) \neq 0$ only for a 25% out of the total $\mathbf{g}$ population and, in this case, for any (h,k,l), the ratio $\frac{|F_s^{\mathrm{sl}}|}{|F_s^{\mathrm{Dy}}|} < 0.3$. We estimate that the tetragonal-like distortion of the reciprocal space contributes to diminishing Δ_{sl} by a factor of $\approx$12. Now, given that the MR in the Dy/Y SL is mainly due to the appearance of superzone band gaps, it is of interest to calculate Δ_{sl}. Thus, using the calculated value for the band gap in bulk Dy,[95] $\Delta_{\mathrm{Dy}} = 0.34$ eV, and Eq. (14), we estimate that $\Delta_{\mathrm{sl}} \approx 0.021$ eV, which means a reduction factor for the superzone band gaps in the SL of $\approx$16. We attribute this large reduction to the tetragonal-like enlargement of the unit lattice cell in the Dy/Y SL, which results from the pronounced chemical modulation. Because of this, only a small fraction of the total $\mathbf{g}$ population meets the condition to produce a band gap[95] in the Dy/Y SL, which ultimately diminishes Δ_{sl} quite significantly when compared to its counterpart Δ_{Dy}.

VI. CONCLUSIONS

Summarizing, we report on evidence that relate a positive magnetoresistance to the onset of fan-type phases in a spin-spiral Dy/Y SL. We find that the maximum positive MR in CPP and CIP geometries show comparable values and a similar nonmonotonic temperature dependence, yielding a maximum value of about $\sim$0.45% at $T = 110$ K. We demonstrate that the positive MR originates in the increasing complexity of the Fourier spectrum of the field-induced modulated magnetic structures, which reflects on the steady increase in the number of superzone band gaps during the magnetization process of the anisotropic spin-spiral magnet. We attribute the suppression of the giant MR in Dy/Y SL to the combined action of chemical modulation and epitaxial strain, which significantly reduce the superzone band gaps. We find that the linear (negative slope) and unsaturated dependence of the MR on H in the high-field limit originates in the scattering of the conduction electrons by magnons. Our study also reveals that the formulation of the *spin-dependent* scattering mechanism in RE metals in terms of the spin-disorder[17] model and the assumption of a *spheroidal Fermi surface* lead to notorious disagreements with the experiment due to their oversimplified nature. Finally, we highlight that positive MR has also been found in Ho/Lu and Ho/Dy SLs and is equally linked to the onset of fan-type magnetic phases.

ACKNOWLEDGMENTS

We wish to thank to N. Benarjee and M. Egilmez for technical assistance. One of us (L.B.) wishes to acknowledge financial support from the EU, Contract No. FP7-PEOPLE-2009-ERG-255669.

*Corresponding author: luisp.benito@googlemail.com

[1] F. Jonietz *et al.*, Science **330**, 1648 (2010).
[2] *Magnetic Properties of Rare Earth Metals*, edited by R. J. Elliott (Plenum, London 1972).
[3] T. Chattopadhyay, Science **264**, 226 (1994).
[4] J. W. A. Robinson, J. D. S. Witt, and M. G. Blamire, Science **329**, 59 (2010).
[5] A. N. Bogdanov and U. K. Rößler, Phys. Rev. Lett. **87**, 037203 (2001).
[6] S. V. Grigoriev, Yu. O. Chetverikov, D. Lott, and A. Schreyer, Phys. Rev. Lett. **100**, 197203 (2008).
[7] G. L. J. A. Rikken, J. Fölling, and P. Wyder, Phys. Rev. Lett. **87**, 236602 (2001).
[8] T. Kasuya, in *Magnetism*, edited by G. T. Rado and H. Suhl (Academic Press, New York, 1966), Vol. IIB.
[9] M. A. Ruderman and C. Kittel, Phys. Rev. **96**, 99 (1954); T. Kasuya, Prog. Theor. Phys. **16**, 45 (1956); K. Yosida, Phys. Rev. **106**, 893 (1957).
[10] A. R. Mackintosh, Phys. Rev. Lett. **9**, 90 (1962).
[11] R. V. Colvin, S. Legvold, and F. H. Spedding, Phys. Rev. **120**, 741 (1960).
[12] M. D. Wilding and E. W. Lee, Proc. Phys. Soc. **85**, 955 (1965).
[13] M. Ellerby, K. A. McEwen, and J. Jensen, Phys. Rev. B **57**, 8416 (1998).
[14] M. Ellerby, K. A. McEwen, E. Bauer, R. Hauser, and J. Jensen, Phys. Rev. B **61**, 6790 (2000).
[15] R. E. Camley and J. Barnaś, Phys. Rev. Lett. **63**, 664 (1989); P. M. Levy, S. Zhang, and A. Fert, *ibid.* **65**, 1643 (1990).
[16] R. J. Elliott and F. A. Wedgwood, Proc. Phys. Soc. **81**, 846 (1963); **84**, 63 (1964).
[17] P. G. de Gennes and J. Friedel, J. Phys. Chem. Solides. **4**, 71 (1958).
[18] V. Sechovsky, L. Havela, L. Jirman, W. Ye, T. Takabatake, H. Fujii, E. Brück, F. R. de Boer, and H. Nakotte, J. Appl. Phys. **70**, 5794 (1991).
[19] K. Prokes, H. Nakotte, E. Brück, F. R. de Boer, L. Havela, V. Sechovsky, and P. Svoboda, IEEE Trans. Magn. **30**, 1214 (1994).
[20] A. R. Mackintosh and L. E. Spanel, Solid State Commun. **2**, 383 (1964).
[21] D. F. McMorrow, P. P. Swaddling, R. A. Cowley, R. C. C. Ward, and M. R. Wells, J. Phys.: Condens. Matter **8**, 6553 (1996).
[22] *Low Level Measurements Handbook*, 6th ed. (Keithley Instruments Inc., Cleveland, 2004).
[23] C. Bell, G. Burnell, D. J. Kang, M. J. Kappers, and M. G. Blamire, Nanotechnol. **14**, 630 (2003).

[24] M. C. Wu, A. Aziz, J. D. S. Witt, M. C. Hickey, M. Ali, C. H. Marrows, B. J. Hickey, and M. G. Blamire, Nanotechnol. **19**, 485305 (2008).

[25] A. K. Burnaham and G. T. Jameson, J. Vac. Sci. Technol. A **5**, 1713 (1987).

[26] D. Weller and D. D. Sarma, Surf. Sci. **171**, L425 (1986).

[27] D. A. Jehan, D. F. McMorrow, R. A. Cowley, R. C. C. Ward, M. R. Wells, N. Hagmann, and K. N. Clausen, Phys. Rev. B **48**, 5594 (1993).

[28] J. A. Simpson, R. A. Cowley, D. F. MoMorrow, R. C. C. Ward, M. R. Wells, C. J. Carlile, and M. A. Adams, J. Phys.: Condens. Matter **8**, L187 (1996).

[29] I. R. Harris and G. V. Raynor, J. Less-Common Met. **17**, 336 (1969).

[30] F. H. Sppeding, A. H. Daane, and K. W. Herrmann, Acta Cryst. **9**, 559 (1956).

[31] D. Sander, J. Phys.: Condens. Matter **16**, R603 (2004).

[32] S. B. Palmer, J. Phys. Chem. Solids **31**, 143 (1970).

[33] D. R. Beherendt, S. Legvold, and F. H. Spedding, Phys. Rev. **109**, 1544 (1958).

[34] F. J. Darnell, Phys. Rev. **130**, 1825 (1963).

[35] A. del Moral and E. W. Lee, J. Phys. C **8**, 3881 (1975); A. del Moral, J. Phys. F: Metal Phys. **8**, 671 (1978).

[36] F. Tsui and C. P. Flynn, Phys. Rev. Lett. **71**, 1462 (1993).

[37] R. W. Erwin, J. J. Rhyne, M. B. Salamon, J. Borchers, S. Sinha, R. Du, J. E. Cunningham, and C. P. Flynn, Phys. Rev. B **35**, 6808 (1987).

[38] K. Dumesnil, C. Dufour, Ph. Mangin, G. Marchal, and M. Hennion, Phys. Rev. B **54**, 6407 (1996).

[39] T. Nagamiya, K. Nagata, and Y. Kitano, Prog. Theor. Phys. **27**, 1253 (1962).

[40] Y. Kitano and T. Nagamiya, Prog. Theor. Phys. **31**, 1 (1964).

[41] R. Herz and H. Kromüller, J. Magn. Magn. Mater. **9**, 273 (1978).

[42] R. M. Bozorth, *Ferromagnetic Materials* (IEEE Press, New York 1993).

[43] C. F. Majkrzak, J. W. Cable, J. Kwo, M. Hong, D. B. McWhan, Y. Yafet, J. V. Waszczak, and C. Vettier, Phys. Rev. Lett. **56**, 2700 (1986).

[44] Y. Yafet, J. Appl. Phys. **61**, 4056 (1987).

[45] J. Kwo, M. Hong, F. J. DiSalvo, J. V. Waszczak, and C. F. Majkrzak, Phys. Rev. B **35**, 7295 (1987).

[46] M. K. Wilkinson, W. C. Koehler, E. O. Wallan, and J. W. Cable, J. Appl. Phys. **32**, 48S (1961).

[47] R. M. Bozorth, Phys. Rev. **50**, 1076 (1936).

[48] J. J. Rhyne and A. E. Clark, J. Appl. Phys. **38**, 1379 (1967).

[49] L. Benito, J. I. Arnaudas, M. Ciria, C. de la Fuente, A. del Moral, R. C. C. Ward, and M. R. Wells, Phys. Rev. B **70**, 052403 (2004).

[50] G. Bertotti, *Hysteresis in Magnetism* (Academic Press, Inc. 1998).

[51] *Ultrathin Magnetic Structures Vol. II*, edited by B. Heinrich and J. A. C. Bland (Springer-Verlag Berlin Heidelberg, 2005), Ch. 2.

[52] C. Isci and S. B. Palmer, J. Phys. F **8**, 247 (1978).

[53] A. V. Andrianov, Yu. P. Gaidukov, A. N. Vasil'ev, and E. Fawcett, J. Magn. Magn. Mater. **97**, 246 (1991).

[54] M. Akhavan, H. A. Blackstead, and P. L. Donoho, Phys. Rev. B **8**, 4258 (1973).

[55] D. W. Boys and S. Legvold, Phys. Rev. **174**, 377 (1968).

[56] P. M. Hall, S. Legvold, and F. H. Spedding, Phys. Rev. **116**, 1446 (1959).

[57] A. del Moral, M. Ciria, J. I. Arnaudas, and C. de la Fuente, Phys. Rev. B **57**, R9471 (1998).

[58] T. Kasuya, Progr. Theoret. Phys. (Kyoto) **22**, 227 (1959).

[59] A. R. Mackintosh and F. A. Smidt Jr., Phys. Lett. **2**, 107 (1962).

[60] L. R. Testardi, J. M. Poate, and H. J. Levinstein, Phys. Rev. B **15**, 2570 (1977).

[61] T. Stobiecki, M. Czapkiewicz, and R. I. Kopcewicz, J. Magn. Magn. Mater. **140-144**, 539 (1995).

[62] K. Fuchs, Proc. Cambridge Phil. Soc. **34**, 100 (1938).

[63] E. H. Sondheimer, Adv. Phys. **1**, 1 (1952).

[64] T. R. McGuire and R. I. Potter, IEEE Trans. Magn. **11**, 1018 (1975).

[65] J. J. Hauser and H. C. Theuerer, Phys. Rev. **134**, A198 (1964).

[66] T. R. Lemberger, I. Hetel, J. W. Knepper, and F. Y. Yang, Phys. Rev. B **76**, 094515 (2007).

[67] R. C. Young, J. Phys. F: Met. Phys. **13**, L239 (1983).

[68] V. N. Antonov, A. Ya. Perlov, P. M. Oppeneer, A. N. Yaresko, and S. V. Halilov, Phys. Rev. Lett. **77**, 5253 (1996).

[69] K. M. Döbrich, A. Bostwick, E. Rotenberg, and G. Kaindl, Phys. Rev. B **81**, 012401 (2010).

[70] K. M. Döbrich, A. Bostwick, J. L. McChesney, K. Rossnagel, E. Rotenberg, and G. Kaindl, Phys. Rev. Lett. **104**, 246401 (2010).

[71] A. V. Andrianov and O. A. Saveleva, Phys. Rev. B **67**, 012405 (2003).

[72] S. J. Crowe, S. B. Dugdale, Zs. Major, M. A. Alam, J. A. Duffy, and S. B. Palmer, Europhys. Lett. **65**, 235 (2004).

[73] M. Ciria, F. J. Castaño, J. L. Diez-Ferrer, J. I. Arnaudas, B. G. Ng, R. C. O'Handley, and C. A. Ross, Phys. Rev. B **80**, 094417 (2009).

[74] J. Wenisch, C. Gould, L. Ebel, J. Storz, K. Pappert, M. J. Schmidt, C. Kumpf, G. Schmidt, K. Brunner, and L. W. Molenkamp, Phys. Rev. Lett. **99**, 077201 (2007).

[75] J. P. Jan, Solid State Phys. **5**, 1 (1957).

[76] S. S. P. Parkin, Appl. Phys. Lett. **63**, 1987 (1993).

[77] A. B. Pippard, *Magnetoresistance in Metals* (Cambridge University Press, Cambridge 1989).

[78] A. R. Mackintosh, Phys. Lett. **4**, 140 (1963).

[79] D. A. Goodings, Phys. Rev. **132**, 542 (1963).

[80] J. Jensen and A. R. Mackintosh, *Rare Earth Magnetism* (Clarendon Press, Oxford, 1991).

[81] A. P. Mihai, J. P. Attané, A. Marty, P. Warin, and Y. Samson, Phys. Rev. B **77**, 060401 (2008).

[82] J. T. Haraldsen and R. S. Fishman, J. Phys.: Condens. Matter **22**, 186002 (2010).

[83] A. K. Majumdar, V. Oestreich, D. Weschenfelder, and F. E. Luborsky, Phys. Rev. B **27**, 5618 (1983).

[84] K. Niira, Phys. Rev. **117**, 129 (1960).

[85] M. Nielsen, H. B. Møller, P. A. Lindgård, and A. R. Mackintosh, Phys. Rev. Lett. **25**, 1451 (1970).

[86] R. M. Nicklow, N. Wakabayashi, M. K. Wilkinson, and R. E. Reed, Phys. Rev. Lett. **26**, 140 (1971).

[87] U. Enz, J. Appl. Phys. **32**, S22 (1961).

[88] W. C. Koehler, J. W. Cable, M. K. Wilkinson, and E. O. Wollan, Phys. Rev. **151**, 414 (1966).

[89] W. C. Koehler, J. W. Cable, H. R. Child, M. K. Wilkinson, and E. O. Wollan, Phys. Rev. **158**, 450 (1967).

[90] T. Nagamiya, J. Appl. Phys. **33**, 1029 (1962).

[91] B. R. Cooper, R. J. Elliott, S. J. Nettel, and H. Suhl, Phys. Rev. **127**, 57 (1962).

[92] K. F. Riley *et al.*, *Mathematical Methods for Phycics and Engineering* (Cambridge University Press, Cambridge, UK 2006).

[93]J. Jensen and A. R. Mackintosh, Phys. Rev. Lett. **64**, 2699 (1990).
[94]T. Kosugia, S. Kawanob, N. Achiwac, A. Onoderad, Y. Nakaie, and N. Yamamoto, Physica B **334**, 365 (2003).
[95]R. E. Watson, A. J. Freeman, and J. P. Dimmock, Phys. Rev. **167**, 497 (1968).
[96]W. C. Koehler, J. W. Cable, E. O. Wallan, and M. K. Wilkinson, Phys. Rev. **126**, 1672 (1962).
[97]I. D. Hughes *et al*., Nature (London) **446**, 650 (2007).
[98]S. B. Palmer, G. J. McIntyre, A. V. Andrianov, and R. J. Melville, J. Magn. Magn. Mater. **177-181**, 1023 (1998).
[99]F. Cinti, A. Cuccoli, and A. Rettori, Phys. Rev. B **78**, 020402 (2008).
[100]V. D. Mello and A. S. Carriço, Surf. Sci. **482-485**, 960 (2001).
[101]T. Kasuya in *Magnetism*, edited by G. T. Rado and H. Suhl (Acedemic, New York, 1966), Vol. IIB.
[102]J. O. Dimmock and A. J. Freeman, Phys. Rev. Lett. **13**, 750 (1964).
[103]A. J. Freeman, J. O. Dimmock, and R. E. Watson, Phys. Rev. Lett. **16**, 94 (1966).
[104]S. C. Keeton and T. L. Loucks, Phys. Rev. **168**, 672 (1968).